Current Variability in Si Nanowire MOSFETs due to Random Dopants in the Source/Drain Regions: A Fully-3D NEGF Simulation Study

Natalia Seoane[1,2], Antonio Martinez[1], Andrew R. Brown[1], *Member, IEEE*, John R. Barker[1] and Asen Asenov[1], *Fellow, IEEE*

[1] Dept. Electronics & Electrical Engineering, University of Glasgow, Glasgow G12 8LT, United Kingdom

[2] Dept. Electronics and Computing Science, Univ. Santiago de Compostela, 15782, Spain

natalia.seoane@usc.es, Tel: +44 141 330 4792, Fax: +44 141 330 4907

Abstract: In this paper we study the impact of random discrete dopants in the source/drain leads on the current variability of a gate-all-around Si nanowire transistor. Due to the strong inhomogeneities of the self-consistent electrostatic potential, a *fully-3D real-space* Non-Equilibrium Green's Function (NEGF) formalism is used. N-channel transistors with random discrete donors in the source/drain regions varying in both numbers and locations have been simulated. We have studied the impact of quasi-bound (QB) states and transmission resonances associated with the attractive potential of the donors on the screening of the impurities and on the current transport. The convergence of the coupled 3D Poisson-NEGF equations for narrow wires with discrete dopants is cumbersome due to the quasi-discrete nature of QB states and resonances of the attractive impurity potential. We present a robust solution strategy dealing with the convergence challenges. Large variations in the on-current and modest variations in the sub-threshold slope are observed in the I_D-V_G characteristics when comparing devices with microscopically different discrete dopant configurations. We have also estimated the access resistance associated with the random dopant regions in the source and the drain leads and find

very good agreement with the resistance estimated from the bulk silicon mobility at the same doping concentration.

INTRODUCTION

Nanowire field-effect transistors (NWTs) attract significant interest as strong contenders for future CMOS applications [1]. Their superior electrostatic integrity offers ultimate-scaling solutions [1]. Indeed, 5 nm channel length Si NWTs have been recently demonstrated experimentally [2]. Strong quantum confinement and tunnelling in such devices calls for full-scale quantum transport (QT) simulations. At the same time, acute atomic scale variability due to discrete dopants, trapped charges, atomic scale interface roughness and body thickness variations necessitate truly 3D solutions.

The statistical variability associated with discrete random dopants, which dominates contemporary MOSFETs, has become a major threat to scaling and integration [3]. Tolerance to very low channel doping makes NWT potentially attractive from a variability point of view. However the statistical variability introduced by random discrete donors in the NWT source/drain (S/D) has never been explored in detail in a full QT context. This is mainly due to the cumbersome convergence when coupling the Non-Equilibrium Green's Function (NEGF) formalism with the Poisson equation in the presence of localised attractive Coulomb potentials and 2D confinement. Nanowires of 3 nm diameter contain, on average, approximately one dopant atom per nanometre of length, for a doping concentration in the range of 10^{20} cm^{-3}. Therefore the potential of a single impurity has a substantial contribution to the total electrostatic potential of a cross-section. The attractive potential creates electron quasi-bound states with zero and resonance transmissions

(Breit-Wigner and Fano type resonances [4]) which contribute to the screening of the donors and influence the current flow. The energy positions and the charging of these states are extremely sensitive to the shape of the self-consistent potential around the impurities. Only recently we have achieved stable convergence in our fully-3D real-space, effective mass NEGF simulator for narrow *n*-channel NWTs with localised donors [5].

Here, we report a systematic quantum transport simulation study of atomic-scale variability in *n*-channel NWTs in the presence of random discrete donors in the S/D regions on a truly statistical scale using the above simulator. The single, positive, ionised donor charges are embedded in the dielectric media of the semiconductor and the polarisation, image charges and screening are taken into account through the solution of Poisson's equation. The self-consistent NEGF simulations capture the contributions of variations in potential, quantum confinement, ionised impurity scattering and related S/D resistance.

Only phonon scattering is excluded from our simulations. However we believe that the inclusion of phonon scattering would have little impact on our results for the following reasons: Experiments and simulations of NWTs with 20 nm channel length and above [6, 7] show a high degree of ballisticity. Therefore we expect that, intrinsically, nanowires with a channel length of 6 nm will operate close to the ballistic limit. In the highly doped source and drain regions the scattering is dominated by impurity scattering, and phonons play a minor role. It has been shown experimentally that the access resistance of the source and drain regions dominates the experimentally measured characteristics of such devices. Also, the inclusion of phonon scattering in a 3D real-space NEGF simulator will add a significant computational load.

In section II we describe the NEGF formalism, focusing on the self-consistent coupling with the 3D Poisson equation and the convergence scheme adopted. Section III presents the simulations results analysing the variations in the I_D-V_G characteristics of the transistor with reference to the energy dependence of the transmission coefficients. We also estimate resistance of the leads associated with the random discrete dopants. The last section summarises the main conclusions of this work.

II TRANSPORT MODEL AND COUPLING WITH THE POISSON EQUATION

The quantum carrier transport is described using the NEGF approach, which is a generalisation of Landauer's formalism [8, 9, 10, 11] for including many body effects. Under certain approximations such as Migdal's theorem [12] (for electron-phonon interaction) and Hartree's approximation [13] (mean field approximation), the NEGF equations can be reduced to closed equations for one particle Green's functions. These approximations have been used extensively in the literature to simulate nanoelectronic devices. The Hamiltonian used in the discretisation of the NEGF equations is an effective-mass Hamiltonian that folds the full crystal interaction into the electron effective masses. The effective masses of the transport valleys are extracted from Tight Binding calculations that capture the dependence of the electron band structure on the nanowire diameter [14]. Due to the small dimensions of the wire cross-section we include only four of the six lowest valleys of the silicon conduction band. The two valleys that have been neglected have transversal masses $0.3m_0$ in the directions perpendicular to the transport direction, resulting in large ground-state energy shifts associated with the transversal confinement. As a result the electron population of these valleys is negligible compared to the other four valleys for the simulated nanowire diameter, temperature and bias conditions.

Sources of incoherent scattering such as phonon interaction, and the corresponding self-energies, are not included in our NEGF simulations. We calculate the correlation matrix, $G^<$, using the recursive algorithm described in [15, 16, 17]. From the correlation matrix, the electron and current densities are calculated by the following equations:

$$n(E,x) = iG^<(E,x,x) \tag{1}$$

$$J(E,x) = -i\frac{e\hbar}{2m}(\nabla - \nabla')G^<(E,x,x')\Big|_{x=x'} \tag{2}$$

The boundary conditions of the Green's function equations at the contacts, which are given through the contact self-energies, are defined using the algorithm described in [18].

Fig. 1 shows the flow chart of our simulator illustrating the computational procedure used to solve the coupled Poisson-NEGF equations. The electrostatic potential and the electron density obtained from a density gradient (DG) solution of the Drift-Diffusion (DD) equations [19] serve as an initial condition for the Poisson-NEGF cycle. The DD solver has Neumann boundary conditions for Poisson's equation in the source and drain instead of the Dirichlet boundary conditions usually used in the DD formalism [20, 21], which matches well with the Green's function boundary conditions. Fig. 2 shows a comparison of the electron densities obtained from NEGF and DG solvers for a nanowire with an impurity located at the middle of the channel. Exceptionally good agreement is obtained between the DG and the NEGF electron distributions after appropriate fitting of the density gradient effective mass. Such close initialisation of the potential distribution at the beginning of the Poisson-NEGF loop reduces drastically the number of NEGF iterations.

After the first Poisson-NEGF iteration the change in electron concentration from

the initial DG solution to the new NEGF solution is moderated by damping. A gradual change in the electron density prevents oscillatory behaviour of the solution around the impurities leading to divergence. The solution instabilities are associated with the extreme sensitivity of the quantum density to the shape of the attractive potential. This is related to the discrete nature of the quasi-bound states and their energy sensitivity to the shape of the potential.

We have found that solving the non-linear Poisson equation results in a much more stable convergence of the Poisson-NEGF system than if the linear version is used. Once a new electron density is obtained from the NEGF solver, a quasi-Fermi level, f_n, is calculated using the new density and the old potential [22]. This quasi-Fermi level is used to update the electron concentration and the Jacobian when solving the non-linear Poisson equation iteratively (see Fig. 1). Adaptive damping is used after the solution of the Poisson equation to limit the change in potential and to improve convergence. The alternate solutions of Poisson and NEGF are iterated until density and current converge.

III RESULTS AND DISCUSSION

1) *The Simulated Devices*

The simulated Si NWTs illustrated in Fig. 3 have a 6 nm undoped channel with 2.2×2.2 nm^2 cross-section, 0.8 nm SiO_2 oxide and 10 nm S/D regions doped at 10^{20} cm^{-3}. The transport in the nanowire occurs in the <100> direction. The nanowire diameter-dependent effective masses are extracted from sp^3d^5 second-neighbour-basis tight-binding calculations [14]. All the simulations in this work have been done at room temperature.

The random dopants have been introduced in a 4 nm region of the S/D leads

between the channel and the continuously doped S/D regions next to the contacts as shown schematically in Fig. 3. Each Si lattice site in these regions is considered and whether this site has a dopant or not is determined using a rejection technique based on the ratio between the doping and the silicon atoms density at that point [23]. The total number of dopants in the discrete dopant regions closely follows a Poisson distribution. The charge of each dopant is distributed to the surrounding nodes of the discretisation mesh using the cloud-in-cell technique. The region with continuous doping between the discrete dopant regions and the contacts guarantees a homogeneous injection into the source/drain from the reservoirs. In our study we have considered a uniform random distribution of donors in the source and drain. In reality, different fabrication conditions, which may include oxidation and segregation [24], may result in a highly non-uniform radial doping distribution. We believe that although the adoption of a more realistic radially non-uniform doping distribution can change the results quantitatively, the qualitative picture of scattering in the access regions will remain unchanged.

2) *Current variability*

Due to the significant computational burden associated the 3D NEGF approach, and its slow convergence in the presence of attractive impurity potentials, the statistical simulation study has been restricted to a small statistical sample of 30 randomly generated device configurations. All simulations were carried out at V_D=1 mV in the linear mode of device operation. Fig. 4 shows, on a linear and logarithmic scale, the current-voltage characteristics of the 30 microscopically different NWTs with different RD configurations. The nanowire with continuous doping (labelled as ‘smooth’ in the figure), and one with no dopants at all in the random dopant regions,

are shown for comparison. At V_G<0.3 V, which marks the transition between the subthreshold and the linear region of the transistor operations, the device configurations with a high concentration of discrete dopants located close to the channel lower the gate barrier potential, leading to a higher current than in the smooth case. At V_G>0.3 V the smooth device always delivers a higher current than in the RD devices. This is mainly associated with the coherent impurity scattering in RD devices, which reduces the current due to partial reflection from the impurity potentials. The degree of backscattering, for a particular RD configuration, depends strongly on the gate voltage. As a consequence, the on-current in 'unlucky' RD devices is reduced to as low as 20% of the current for the smooth device. A particular configuration may have low scattering at low V_G and high scattering at high V_G, or vice versa, relative to other configurations. This sensitivity to the gate voltage is a result of the relative proximity of the discrete dopants to the tail of the channel potential barrier and lead to a crossing of the I_D-V_G curves as can be seen in Fig.4.

There is a variation in the sub-threshold slope of the I_D-V_G curves produced by the different atomistic configurations. Devices with configurations of dopants close to the central axis of the wire, far from the SiO_2 interfaces, will have relatively poor electrostatic control compared with devices with dopants distributed closer to the interfaces and to the channel/source and channel/drain junctions. In addition to the subthreshold slope variation due purely to electrostatics, which have been observed in drift-diffusion simulations, there is an additional contribution from the varying degrees of source-to-drain tunnelling.

In the presence of RD in the access regions the average magnitude of the on-current drops by 48% compared to the uniformly doped purely ballistic device. More importantly, despite the absence of channel doping the standard deviation of the on-

current is extremely high at 38%. This is beyond the variability level of tolerance for the present circuit design practices. Either the design practices need to be changed to cope with such levels of variability or Schottky source drain contacts have to be considered to remove the doping granularity issues from the extensions.

3) *Transmission coefficient based analysis*

The physical effects shaping the impact of the discreteness of the donors on the current-voltage characteristics can be explained qualitatively using the transmission coefficients, which are directly related to the current through the well-known Landauer formula [25],

$$J = \int T(\varepsilon)\left(f_S(\varepsilon) - f_D(\varepsilon)\right) d\varepsilon \tag{3}$$

relating the transmission coefficient T and the Fermi distributions in the S/D, $f_S(\varepsilon)/f_D(\varepsilon)$.

At V_G=0.1 V, we have investigated the behaviour of the device configurations with: the lowest current (L), the median current (M) and the highest current (H). The number and positions of the impurities in each one of the three devices are presented in Table I. Fig. 5 shows the 3D self-consistent electrostatic potential for the L (top), M (middle) and H (bottom) cases, illustrating the localised potential features created by the discrete dopants. The trend observed in the figure is an increase in the current when the impurities are closer to the channel as they weaken the channel barrier potential. The lowest current device has only two discrete dopants, one located in the source and the other in the drain. Both dopants are very close to the Si/SiO_2 interface and far away from the channel. The median current device has three impurities, one placed in the source close to the interface, and the other two in the drain close to the interface and to each other, but a little off from the channel. Finally, the highest current device has three impurities which are located very close to the channel, two of

them in the source and the third one in the drain. The electron density and the potential along the middle of the channel for the smooth device and for the L, M and H devices are shown in Fig. 6. The figure shows a narrowing and lowering of the barrier when going from the lowest to the highest current devices. The corresponding electron density for the narrowest barrier has higher maximum value and penetrates more into the channel. The transmission coefficients as a function of the energy are shown in Fig. 7. The transmission of the highest current device, which has the lowest barrier height, rises first and the other transmission coefficients are shifted to higher energies in the same order as their increasing barrier height. The corresponding current behaviour follows from Landauer's expression in Eq. 3.

At a higher gate bias of V_G=0.4 V we repeat the analysis by selecting the three devices with the lowest (L), median (M) and highest current (H), which are different devices from those at V_G=0.1 V. The number and position of the impurities for the three cases is presented in Table 2. The corresponding 3D self-consistent electrostatic potential distributions are shown in Fig. 8 (although not all the impurities are evident in the figure). The device with the shortest effective channel length exhibits the largest current. This is clear from Fig. 9, which shows for the electron concentration and self-consistent electrostatic potential along the middle of the channel. The device with the largest current has six dopants in the source, producing a region of average dopant concentration much larger than the dopant concentration of the continuously doped smooth device. Fig. 10 shows the transmission coefficients for the three RD devices and for the smooth device presented as a reference.

For the highest current device the shape of the self-consistent potential around some impurities produces Fano-type resonances as seen in Fig. 10. These result in zero transmission at the resonance energies and can be interpreted as back scattering

for the corresponding electrons. The electrons at these resonant energies (or quasi-bound states) are the main source of the screening of the impurity potential. For the other two devices we have transmission resonance peaks due to the inverted sombrero shape of the self-consistent potential of the impurities (see Fig.9). The same analysis carried out for the low gate bias using the Landauer formula can be used to correlate the transmission coefficients to the electron current. Note that the transmission for the smooth device has a stair-type characteristic as expected. Therefore, the irregular shape and dips in the transmission for the devices with discrete impurities can be interpreted as a fraction of carriers being reflected back or back scattered. This feature is not visible at lower gate bias because of the dominant reflection of the carriers by the channel barrier potential.

4) *Resistance of the RD regions*

Finally we estimate the resistance/conductance of the RD regions associated with the impurity scattering by self-averaging their impact on the nanowire current in the linear regime of operation. Estimates of the conductance of a 200 nm long silicon wire based on the NEGF + DFT (density functional theory) formalism are carried out in [26] by averaging the conductance over every realisation of disorder, i.e. spatial discrete dopant configuration.

The on-current in the case of the random dopant devices is always lower than in the smooth case. This reduction in current is attributed to an increase in the access resistance due to scattering of the electron wave packet by the coulomb potential of the discrete impurities, which is therefore included in an “ab initio” fashion. Here, we estimate the average resistance of the RD regions introduced by the “ab initio” impurity scattering from the random discrete dopants by subtracting the resistance of the smooth device (V_D/I_D at a given gate voltage) from the average resistance of the

random dopant devices.

The average access resistance is calculated from the difference between the average current of the random dopant devices and the smooth (purely ballistic) device at gate voltages of V_G=0.5 and 0.6 V. This selection reduces the inaccuracy associated with modest random threshold voltage shifts that are well pronounced in the subthreshold region. The calculated average resistances at V_G=0.5 and 0.6 V are 3.64×10^4 and 2.17×10^4 Ω for V_G=0.5 and 0.6 V respectively. The corresponding smooth device resistances are 1.96×10^4 and 1.04×10^4 Ω. Therefore the estimated access resistance of the RD regions associated with 'ab initio' impurity scattering is 1.68×10^4 and 1.13×10^4 Ω respectively. The slight decrease in the resistance at the higher gate voltage is due to the gate modulation of the electron concentration at the gate edges of the source/drain extensions.

The theoretical bulk resistance is calculated for the geometry of the RD extensions which have a cross-section s=2.2×2.2 nm^2 and length l=8 nm. This resistance (R) is calculated from the resistivity $\rho=7.70\times10^{-4}$ Ωcm [27] of n-type silicon corresponding to a doping concentration of 10^{20}cm^{-3} at 300 K. At such high doping concentration, the phonon scattering contribution to the resistance is negligible, as estimated using Matthiessen's rule and the room temperature phonon-limited mobility. The value of the calculated resistance using the expression $R=\rho l/s$ is R≈1.27x10^4 Ω. This value matches very well the resistance estimated from the ensemble averaging of the impurity scattering from each 'atomistic' device. This suggests that when the coherent transport (interference) from the different I_D-V_G curves are averaged out, NEGF can intrinsically reproduce the classical ionised impurity scattering [28]. Also each device contains, in general, several dopants with randomly generated positions, which produce constructive and destructive interference effects unlike the case of one single

dopant which creates less disorder.

IV CONCLUSIONS

In this paper we have used a full 3D Non-Equilibrium Green's Function formalism to estimate the variability in the I_D-V_G characteristics of a future-generation Si nanowire transistor induced by random dopants (RD) in the source/drain extensions. The self-consistent electrostatic potential shows strong inhomogeneities which can only be captured in a full three-dimensional real-space description of the carrier transport. These inhomogeneities are very unlikely to be properly captured in a quasi-one-dimensional assessment of the transport.

In the sub-threshold regime there is a noticeable variation in the sub-threshold slope due to the presence of random dopants in the source/drain. Configurations with dopants placed close to the channel weaken the gate potential barrier leading to a sub-threshold current larger than the uniform smooth device current. As a result of the access resistance associated with the RD regions the average magnitude of the on-current is reduced by 48% compared to the uniformly doped purely ballistic device. Despite the absence of channel doping the standard deviation of the on-current is extremely high at 38%.

Common features in the transmission coefficients are the presence of back-scattering and resonances, including very localised zero-transmission resonances coming from unscreened coulomb wells.

Finally, we have estimated the resistance associated with the random dopants. This resistance is in very good agreement with the theoretical bulk resistance for Silicon at the same doping concentration.

REFERENCES

[1] K. H. Yeo, K. H. Cho, M. Li, S. D. Suk, Y. Yeoh, M. S. Kim, H. Bae, Ji-M. Lee, S. K. Sung, J. Seo, B. Park, D. W. Kim, D. Park, and W. S. Lee, "Gate-all-around single silicon nanowire MOSFET with 7 nm width for SONOS NAND flash memory", *2008 Symposium on VLSI Technology Digest of Technical Papers*, p.138, 2008.

[2] T. Y. Liow, K. M. Tan, R. T. P. Lee, M. Zhu, B. L. H. Tan, G. S. Samudra, N. Balasubramanian, and Y. C. Yeo, "5 nm gate length nanowire-FETs and planar UTB-FETs with pure germanium source/drain stressors and laser-free melt-enhanced dopant (MeltED) diffusion and activation technique", *2008 Symposium on VLSI Technology Digest of Technical Papers*, p.36, 2008.

[3] G. Roy, A. R. Brown, F. Adamu-Lema, S. Roy and A. Asenov, "Simulation study of individual and combined sources of intrinsic parameter fluctuations in conventional nano-MOSFETs", *IEEE Trans. on Electron Devices*, Vol.53, No.12, p.3063, 2006.

[4] J. H. Bardarson, I. Magnusdottir, G. Gudmundsdottir, C. S. Tang, A. Manolescu and V. Gudmundsson, "Coherent electronic transport in a multimode quantum channel with Gaussian-type scatterers", *Phys. Rev. B*, Vol.70, p.245308, 2004.

[5] A. Martinez, J. R. Barker, A. R. Brown, N. Seoane and A. Asenov, "Simulation of impurities with an attractive potential in fully 3D real space Non-Equilibrium Green's Function quantum transport simulations", *International Conference on Simulation of Semiconductor Processes and Devices (SISPAD)*, p.341, 2008.

[6] W. Lu, J. Xiang, B. P. Timko, Y. Wu and C. M. Liebert, "One-dimensional hole gas in germanium/silicon nanowire heterostructures", *Proc. Natl. Acad. Sci. U.S.A.*, Vol.102, p.10046, 2005.

[7] K. H. Cho et al., "Experimental evidence of ballistic transport in cylindrical

gate-all-around twin silicon nanowire metal-oxide-semiconductor field effect transistors", *App. Phys. Lett.*, Vol.92, p.052102, 2008.

[8] R. Landauer, "Electrical resistance of disordered one-dimensional lattices", *Phil. Mag*., Vol.21, p.863, 1970.

[9] M. Buttiker, "Symmetry of electrical conduction", *IBM J. Res. Dev*., Vol.32, p.317, 1988.

[10] H. L. Engquist. and P. W. Anderson, "Definition and measurements of the electrical and thermal resistances", *Phys. Rev. B*, Vol.24, p.1151, 1981.

[11] Y. Imry and R. Landauer, "Conductance viewed as transmission", *Rev. Mod. Phys*, Vol.71, p.306, 1999.

[12] A. B. Migdal, Translation: *Soviet physics-JEPT*, Vol.7, p.996, 1958.

[13] J. C. Inkson, "Many-body theory of solids", *Plenum Press*, p.128, 1984.

[14] K. Nehari, N. Cavassilas, J. L. Autran, 1, M. Bescond, D. Munteanu and M. Lannoo, "Influence of band structure on electron ballistic transport in silicon nanowire MOSFET's: an atomistic study", *Solid-State Electronics*, Vol.50, p.716, 2006.

[15] R. Lake, G. Klimeck, R. C. Bowen and D. Jovanovic, "Single and multiband modeling of quantum electron transport through layered semiconductor devices", *J. App. Phys*., Vol.81, p.7845, 1997.

[16] A. Svizhenko, M. P. Anantram, T. R. Govindan, B. Biegel and R. Venugopal, "Two dimensional quantum mechanical modelling of nanotransistors", *J. Apps. Phys.*, Vol.91, p.2343, 2002.

[17] M. P. Anantram, A. Svizhenko and A. Martinez, "Erratum: Two-dimensional quantum mechanical modelling of nanotransistors", *J. App. Phys*., Vol.100, p.119903, 2006.

[18] R. Venugopal, Z. Ren, S. Datta, D. Jovanovic and M. S. Lundstrom, "Simulating quantum transport in nanoscale transistors: Real versus mode-space approaches", *J. Appl. Phys.*, Vol.92, p.3730, 2002.

[19] A. Asenov, G. Slavcheva, A. R. Brown, J. H. Davies and S. Saini, "Increase in the random dopant induced threshold fluctuations and lowering in sub-100 nm MOSFETs due to quantum effects: a 3-D density-gradient simulation study", *IEEE Trans. Electron Dev.*, Vol.48, No.4, p.722, 2001.

[20] A. R. Brown, A. Martinez, M. Bescond and A. Asenov, "Nanowire MOSFET variability: a 3D density gradient versus NEGF approach", *Silicon Nanoelectronics Workshop, 10-11 June, Kyoto, Japan*, p.127, 2007.

[21] C. Riddet, A. R. Brown, S. Roy and A. Asenov, "Boundary conditions for density gradient corrections in 3D Monte Carlo simulations", *Journal of Computational Electronics*, Vol.7, p.231, 2008.

[22] M. P. Anantram and A. Svizhenko, "Multidimensional modelling of Nanotransistors", *IEEE Trans. Electron Devices*, Vol.54, p.2100, 2007.

[23] D. J. Frank, Y. Taur, M. Ieong and H.-S. P. Wong, "Monte Carlo modeling of threshold variation due to dopant fluctuations", *Symposium on VLSI Technology Dig. Techn. Papers*, p.169, 1999.

[24] M. V. Fernandez-Serra, Ch. Adessi and X. Blase, "Surface segregation and backscattering in doped silicon nanowires", *Phys. Rev. Lett.*, Vol.96. p.166805, 2006.

[25] Y. Meir and N. S. Wingreen, "Landauer formula for the current through an interacting electron region", *Phys. Rev. Lett.*, Vol.68. p.2512, 1992.

[26] T. Markussen, R. Rurali, A-P. Jauho and M. Brandbyge, "Transport in silicon nanowires: role of radial dopant profile", *Journal of Computational Electronics*,

Vol.7, p.324, 2008.

[27] Properties of Crystaline Silicon, *ed. by Robert Hull, INSPEC publications,* 1999.

[28] S. Datta, “Quantum transport, atom to transistor”, *Cambridge University Press*, 2005.

Table and Figure captions:

Table 1. Location of the discrete dopants for the three cases with lowest, median and highest currents, at V_G=0.1 V. The channel of the device is between 10 nm and 16 nm in the *x*-direction. In the *y*- and *z*-directions the silicon body is 2.2 nm thick. The regions of the source and drain where discrete random dopants are placed extend for 4 nm on either side of the channel.

Table 2. Location of the discrete dopants for the three cases with lowest, median and highest currents, at V_G=0.4 V. The channel of the device is between 10 nm and 16 nm in the *x*-direction. In the *y*- and *z*-directions the silicon body is 2.2 nm thick. The regions of the source and drain where discrete random dopants are placed extend for 4 nm on either side of the channel.

Fig. 1. Flow chart of the 3D Poisson-NEGF solution methodology.

Fig. 2. Comparison of the electron concentration from density gradient and NEGF in the nanowire transistor with a donor impurity in the middle of the channel. Two profiles are shown: (top) along the centre of the nanowire from source to drain; (bottom) transversally from top to bottom interfaces through the dopant location. The density gradient effective mass is 0.19 m_0. The bias conditions are V_D=1 mV and V_G=0.7 V.

Fig. 3. Schematic view of the nanowire transistor for the case of *random dopants* in the source and drain.

Fig. 4. I_D-V_G characteristics of the nanowire transistor with *random dopants* in the source and drain. The full black line is for a device with no dopants in the white 'atomistic' regions of Fig. 3.

Fig. 5. Potential for the *random dopants* devices with lowest, median and highest

current at V_G=0.1 V. From top to bottom, the lowest current (L), median current (M) and highest current (H) devices are represented.

Fig. 6. Density and potential along the nanowire at V_G=0.1 V for the smooth and the three *random dopant* devices.

Fig. 7. Transmission coefficients at V_G=0.1 V for the smooth and three *random dopant* devices. The early start of the transmission of the highest current device is a consequence of the impurities close to the channel (see Fig. 5).

Fig. 8. Potential for the lowest, median and highest current of the *random dopant* devices at V_G=0.4 V. From top to bottom, the lowest current (L), median current (M) and highest current (H) devices are represented.

Fig. 9. Density and potential along the wire at V_G=0.4 V for the smooth and the three *random dopant* devices.

Fig. 10. Transmission coefficients at V_G=0.4 V for the smooth and three *random dopant* devices.

Table 1:

Random Dopant configuration V_G=0.1 V	N. of dopants	Dopant position		
		X (nm)	Y (nm)	Z (nm)
Lowest current	2	6.79	1.09	0.27
		18.73	1.90	2.17
Median current	3	8.96	1.09	1.90
		17.10	1.36	2.17
		17.65	1.38	1.63
Highest current	3	9.23	0.00	1.63
		9.77	0.27	0.81
		16.56	0.00	0.81

Table 2:

Random Dopant configuration V_G=0.4 V	N. of dopants	Dopant position		
		X (nm)	Y (nm)	Z (nm)
Lowest current	2	6.65	2.04	2.04
		9.77	0.81	0.81
Median current	3	7.06	0.54	0.00
		9.64	0.95	0.13
		18.73	0.81	0.54
Highest current	9	6.52	1.09	2.17
		7.33	0.00	0.27
		7.33	1.35	1.09
		7.87	0.81	1.09
		8.55	0.68	0.41
		8.96	0.81	1.63
		16.70	1.49	0.14
		18.46	1.63	1.09
		19.96	0.41	0.68

Figure 1

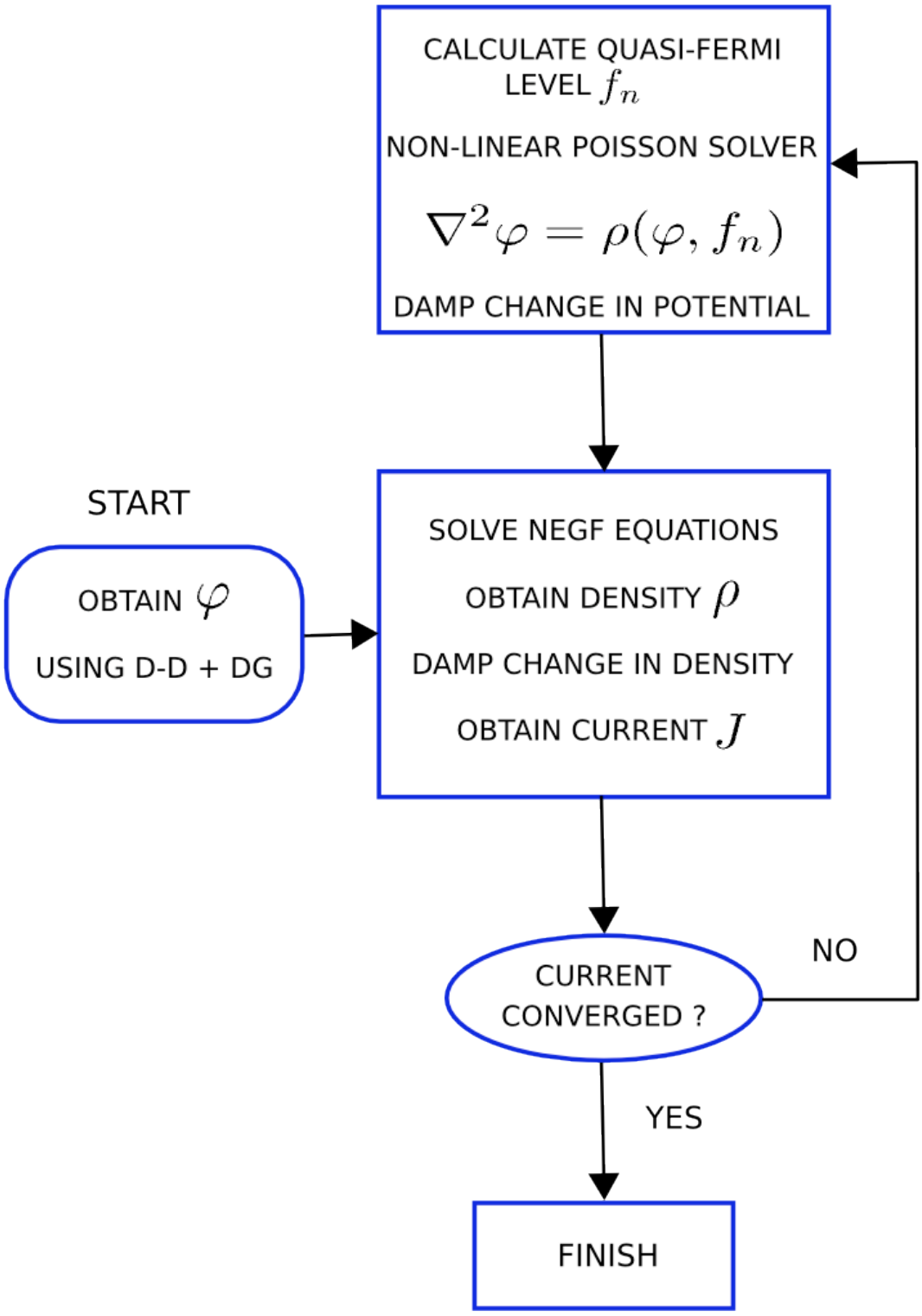
CALCULATE QUASI-FERMI LEVEL f_n
NON-LINEAR POISSON SOLVER
$\nabla^2\varphi = \rho(\varphi, f_n)$
DAMP CHANGE IN POTENTIAL
START
OBTAIN φ
USING D-D + DG
SOLVE NEGF EQUATIONS
OBTAIN DENSITY ρ
DAMP CHANGE IN DENSITY
OBTAIN CURRENT J
CURRENT CONVERGED ?
NO
YES
FINISH

Figure 2

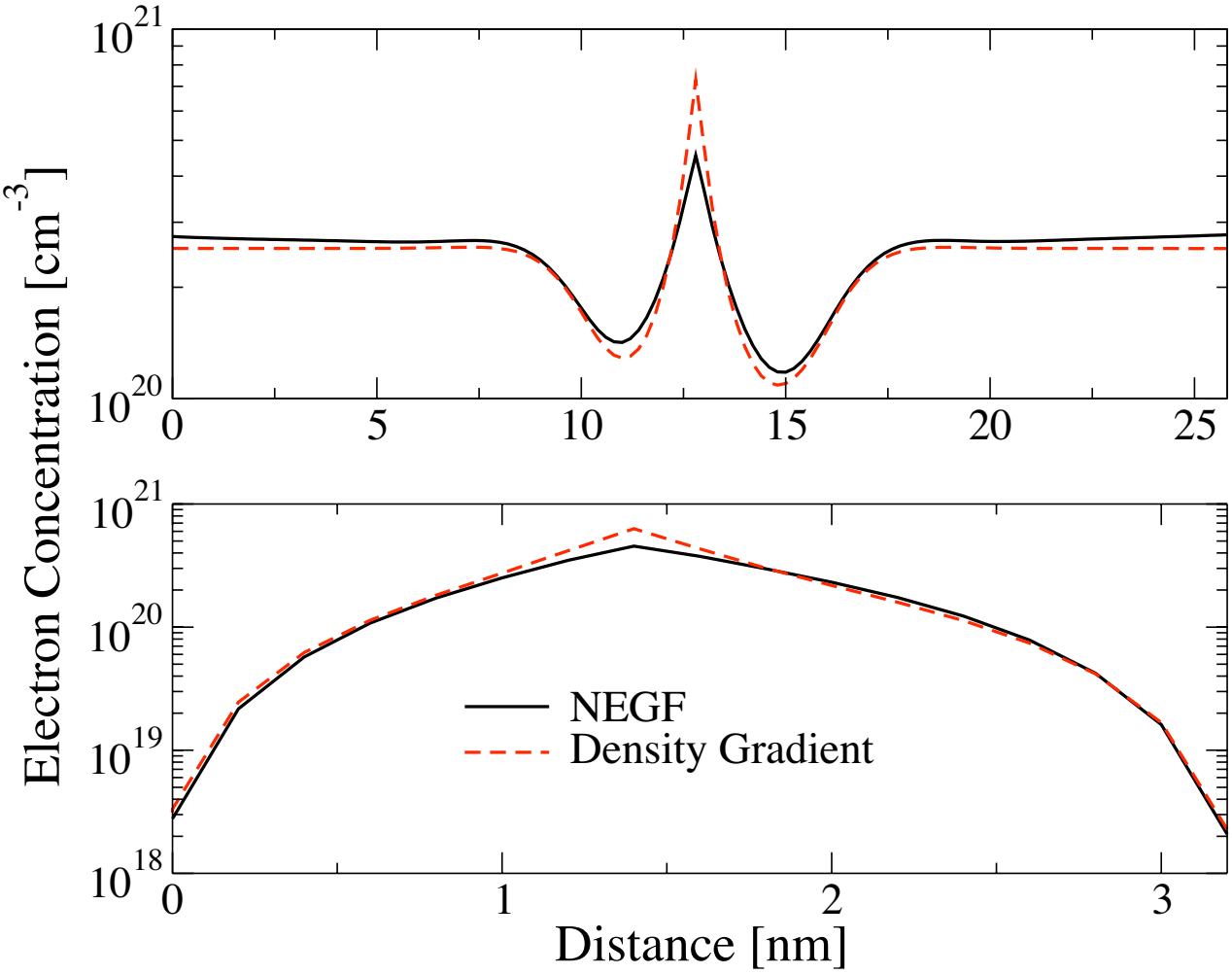
Electron Concentration [cm^{-3}]
10^{21}
10^{20}
0
5
10
15
20
25
10^{21}
10^{20}
10^{19}
10^{18}
0
1
2
3
NEGF
Density Gradient
Distance [nm]

Figure 3

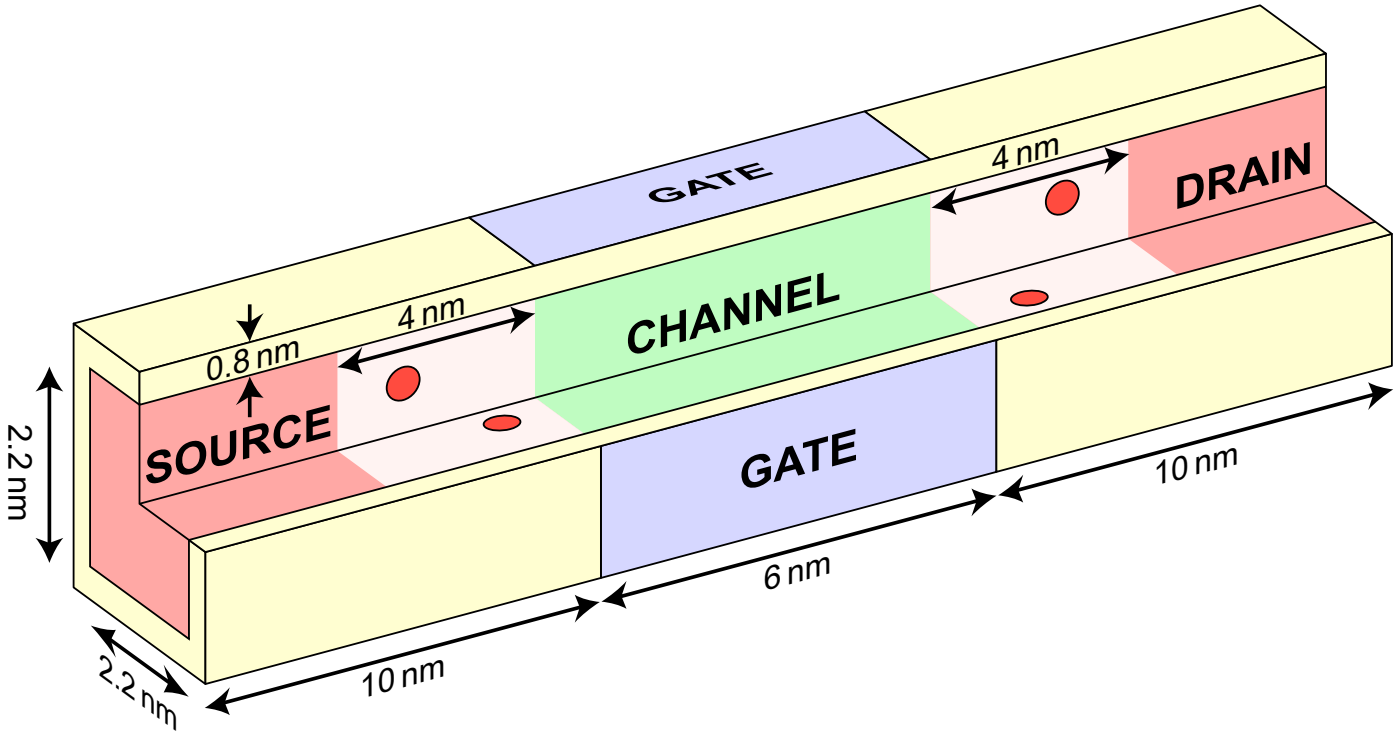
GATE
4 nm
DRAIN
0.8 nm
4 nm
CHANNEL
SOURCE
GATE
10 nm
2.2 nm
6 nm
10 nm
2.2 nm

Figure 4

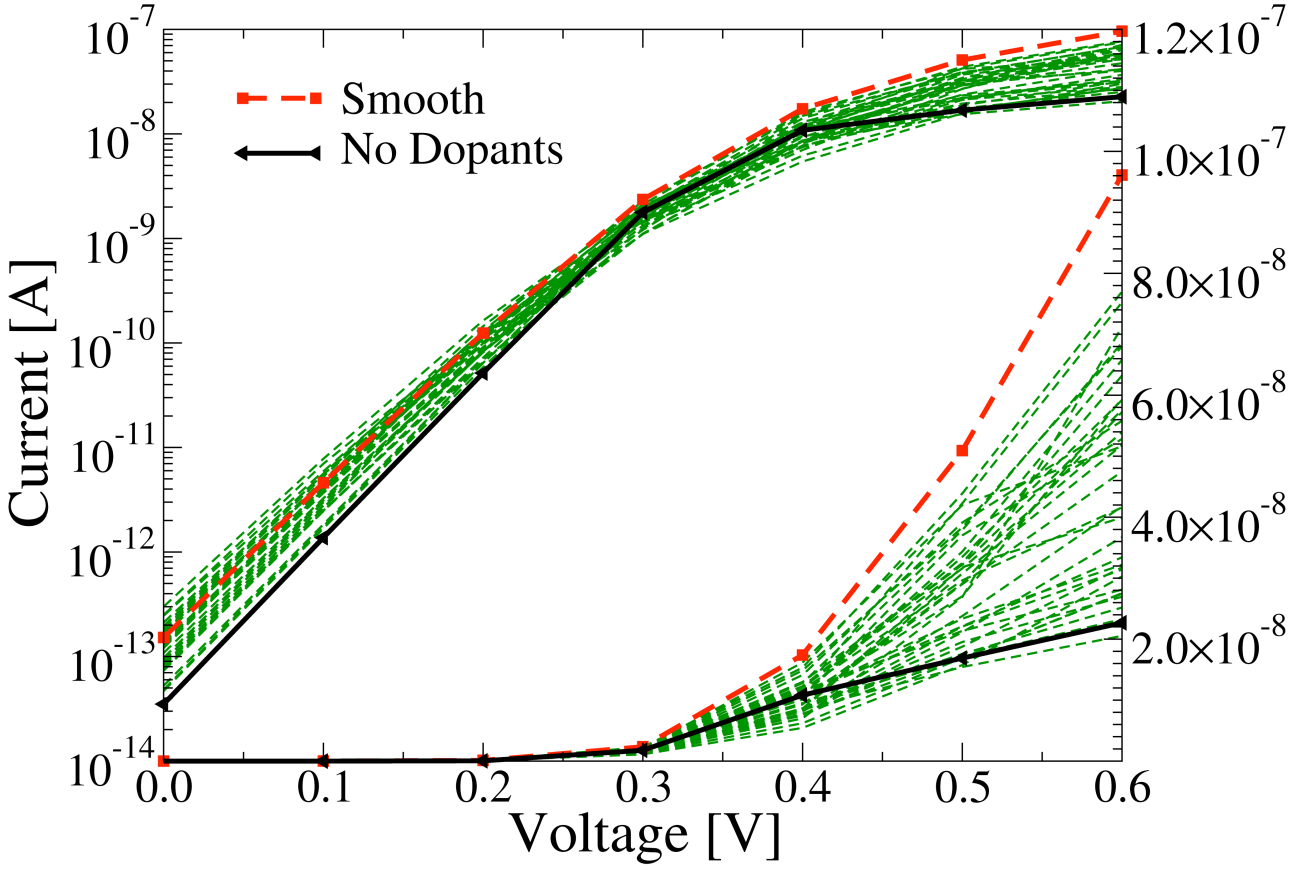
Smooth
No Dopants
Current [A]
Voltage [V]
10^-7
10^-8
10^-9
10^-10
10^-11
10^-12
10^-13
10^-14
1.2×10^-7
1.0×10^-7
8.0×10^-8
6.0×10^-8
4.0×10^-8
2.0×10^-8
0.0
0.1
0.2
0.3
0.4
0.5
0.6

Figure 5

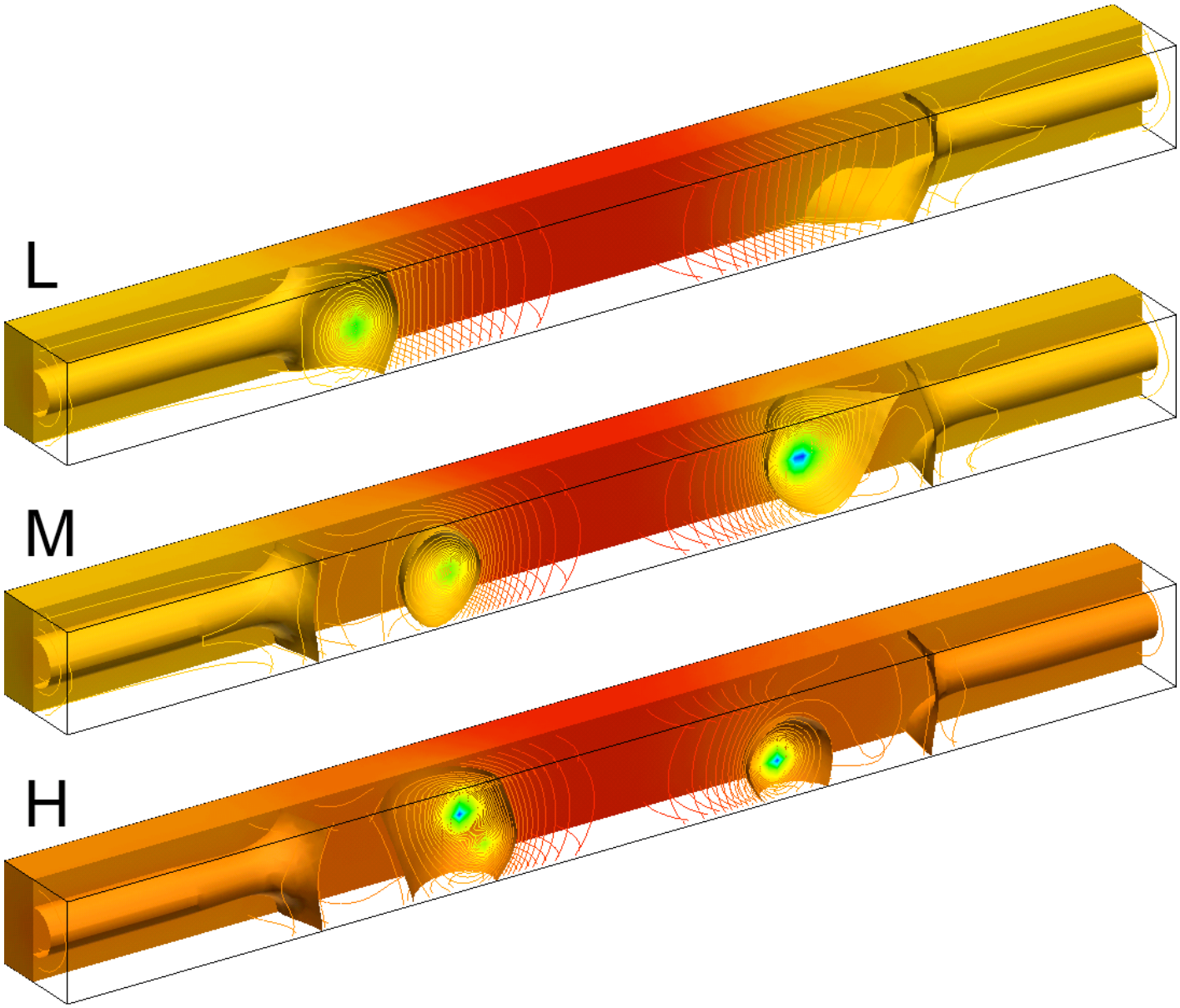

Figure 6

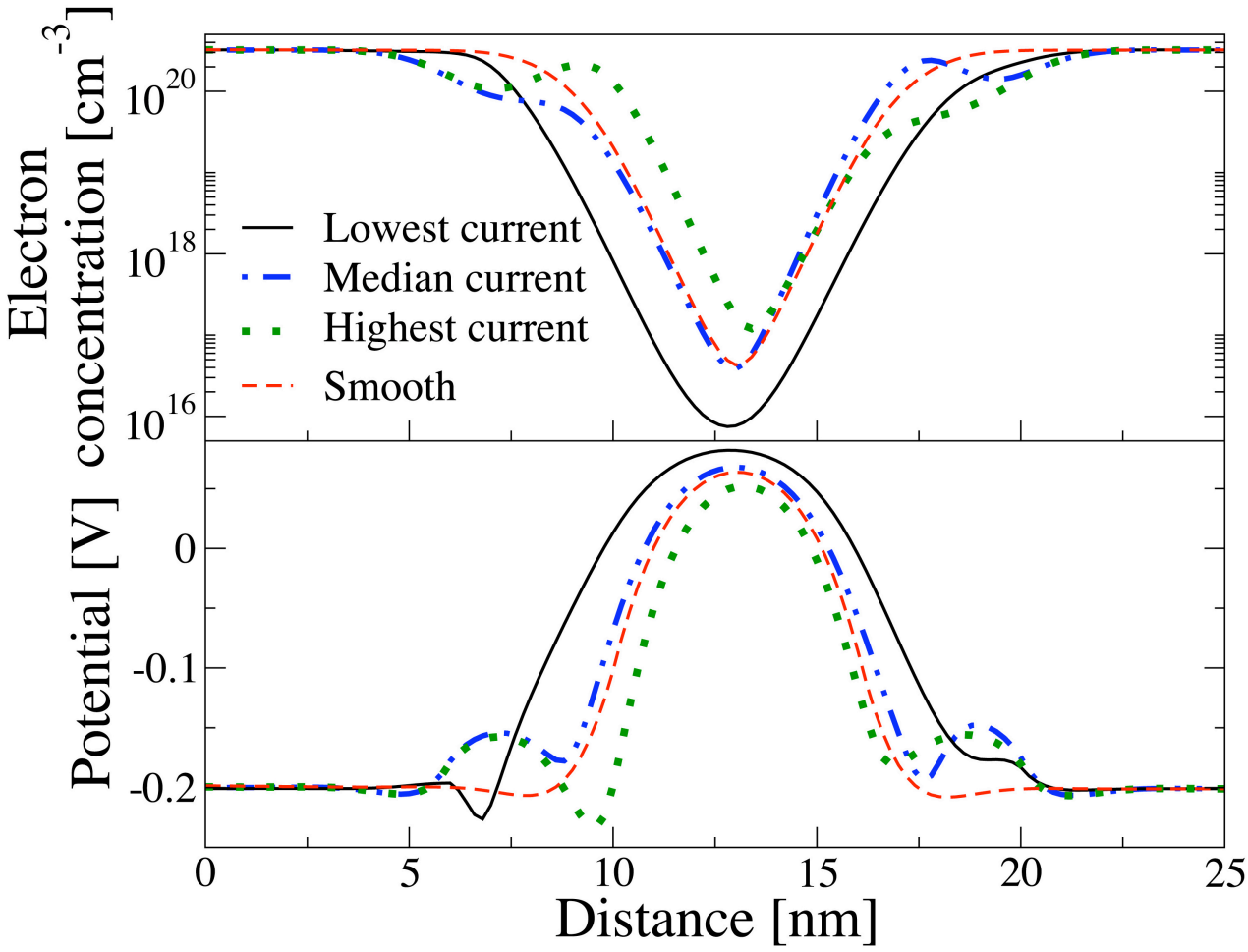
Electron concentration [cm^{-3}]
10^{20}
10^{18}
10^{16}
Lowest current
Median current
Highest current
Smooth
Potential [V]
0
-0.1
-0.2
0
5
10
15
20
25
Distance [nm]

Figure 7

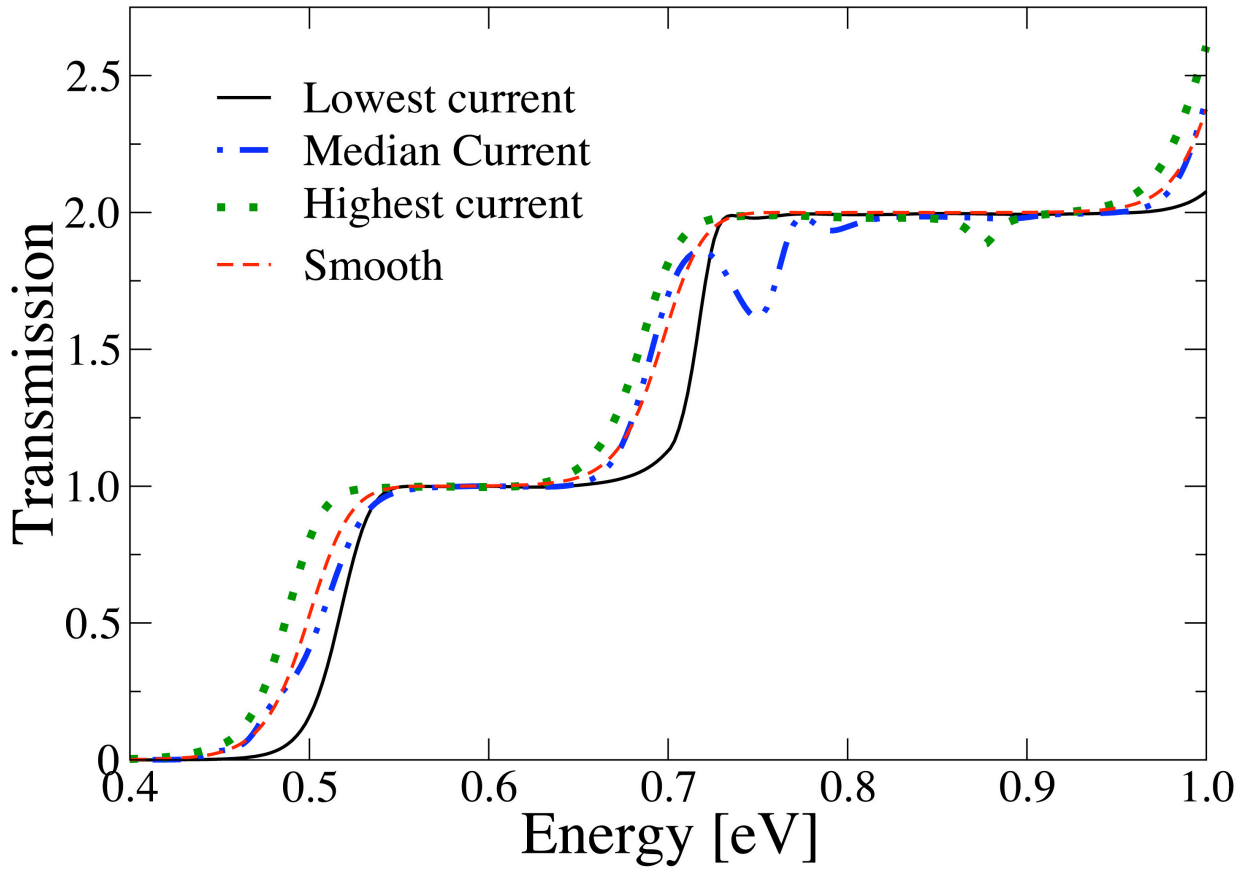
Lowest current
Median Current
Highest current
Smooth
Transmission
Energy [eV]
0
0.5
1.0
1.5
2.0
2.5
0.4
0.5
0.6
0.7
0.8
0.9
1.0

Figure 8

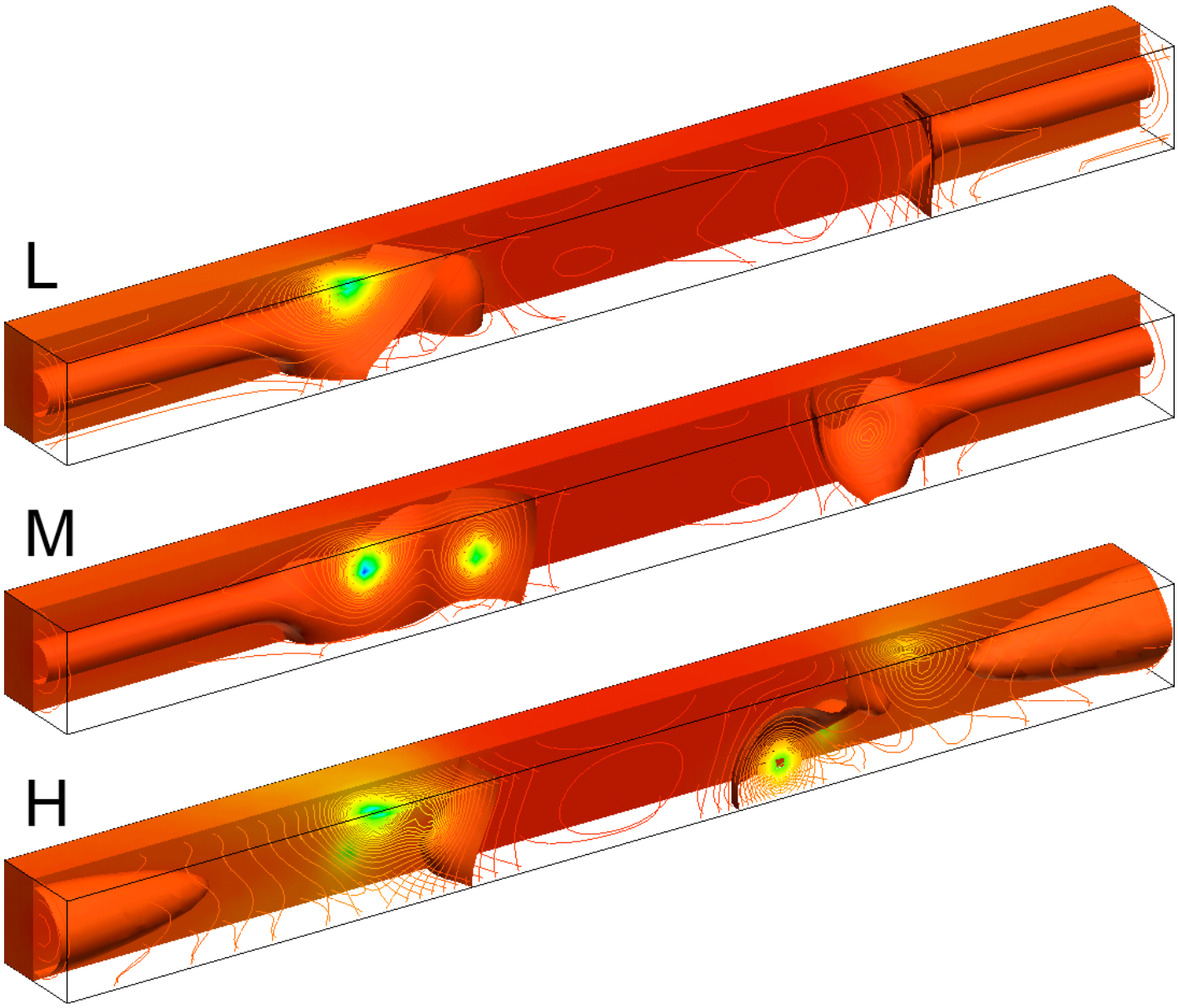

Figure 9

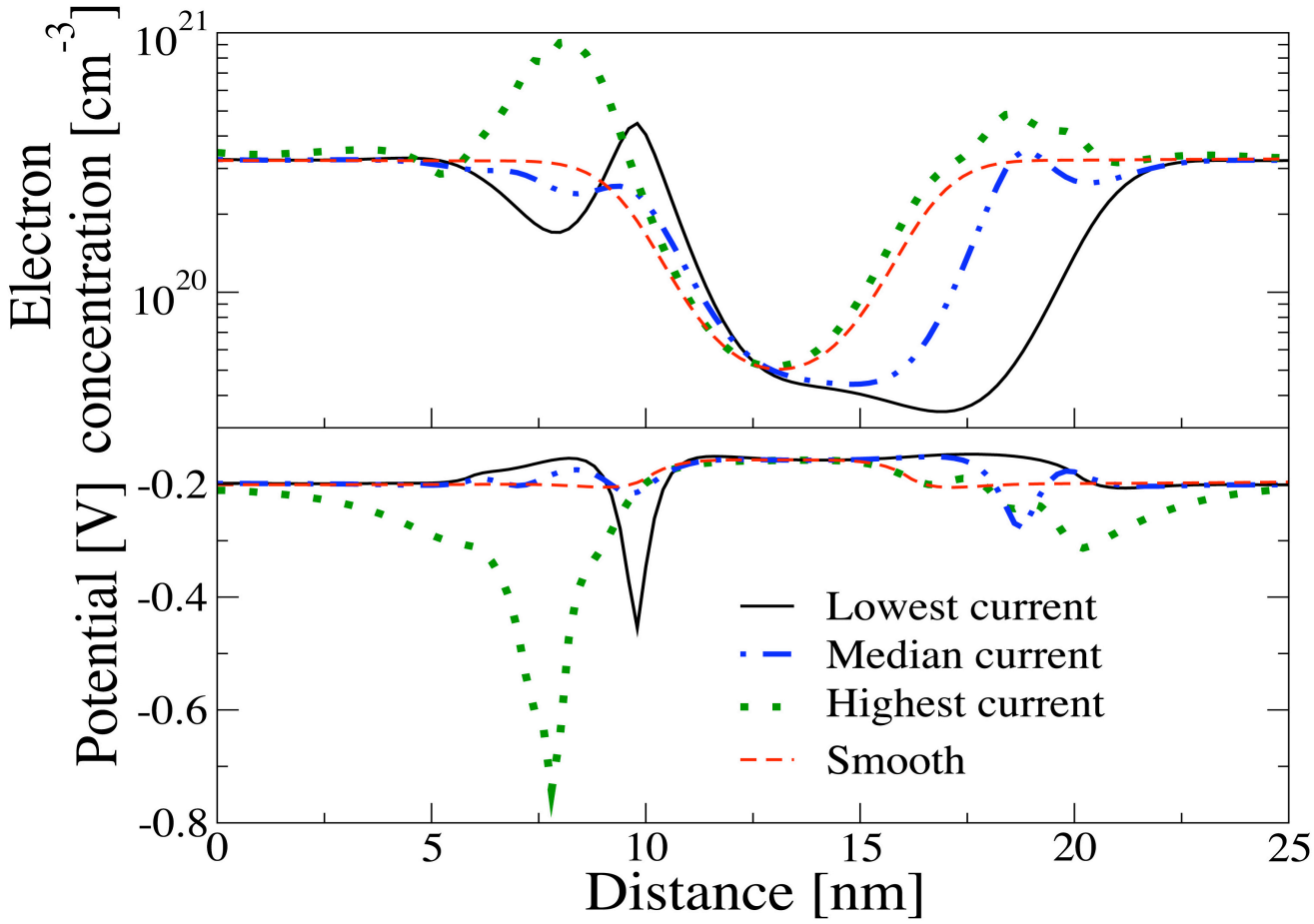
Electron concentration [cm^{-3}]
10^{21}
10^{20}
Potential [V]
-0.2
-0.4
-0.6
-0.8
0
5
10
15
20
25
Distance [nm]
Lowest current
Median current
Highest current
Smooth

Figure 10

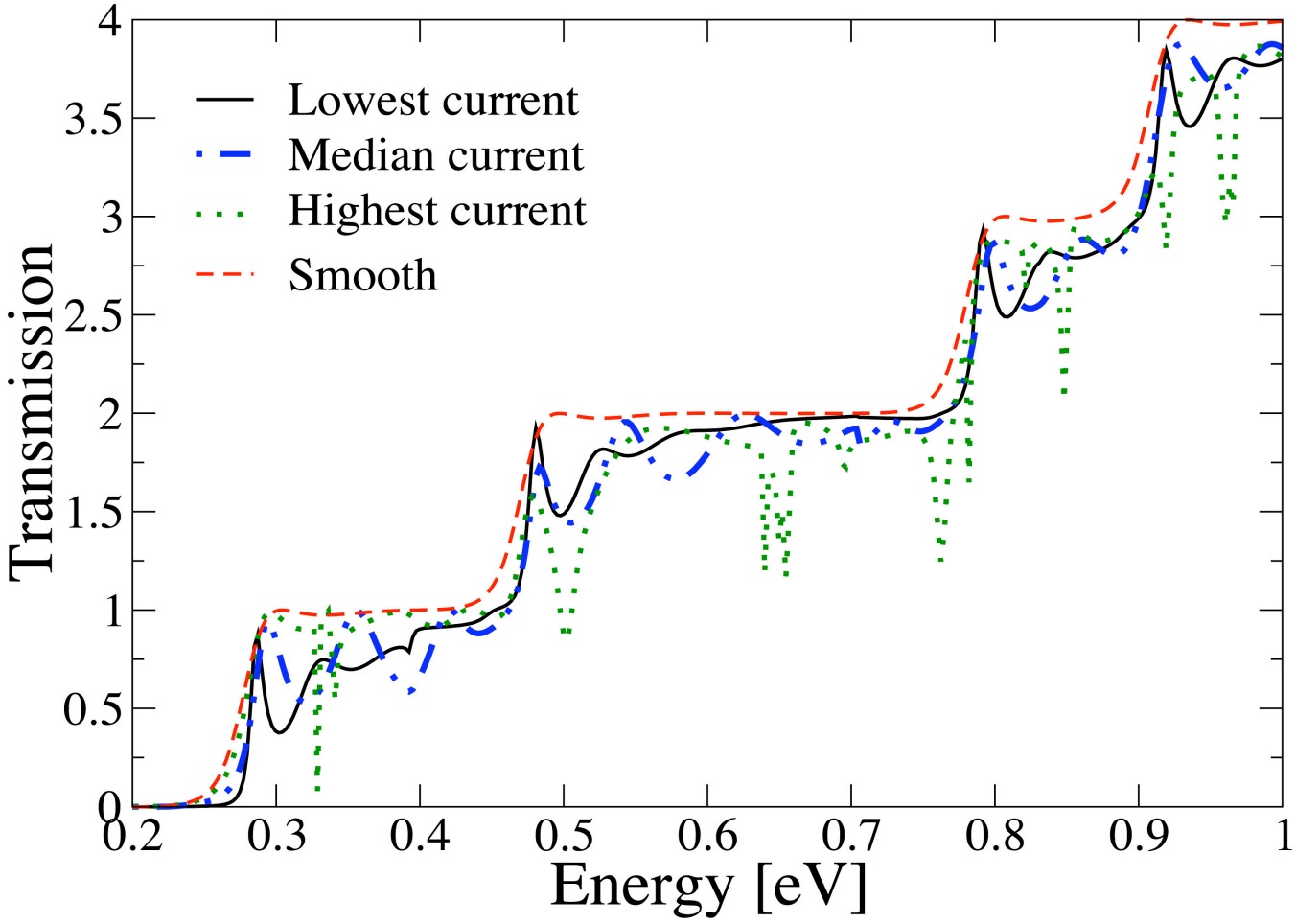
Lowest current
Median current
Highest current
Smooth
Transmission
Energy [eV]
0
0.5
1
1.5
2
2.5
3
3.5
4
0.2
0.3
0.4
0.5
0.6
0.7
0.8
0.9
1